UV Resonance Raman Investigation of the Conformations and Lowest Energy Allowed Electronic Excited States of Tri- and Tetraalanine: Charge Transfer Transitions

Bhavya Sharma and Sanford A. Asher*

Department of Chemistry, University of Pittsburgh, 219 Parkman Avenue, Pittsburgh, Pennsylvania 15260

Received: January 15, 2010; Revised Manuscript Received: March 16, 2010

UV resonance Raman excitation profiles and Raman depolarization ratios were measured for trialanine and tetraalanine between 198 and 210 nm. Excitation within the $\pi \rightarrow \pi^*$ electronic transitions of the peptide bond results in UVRR spectra dominated by amide peptide bond vibrations. In addition to the resonance enhancement of the normal amide vibrations, we find enhancement of the symmetric terminal COO^- vibration. The Ala_3 UVRR $AmIII_3$ band frequencies indicate that poly-proline II and 2.5_1 helix conformations and type II turns are present in solution. We also find that the conformation of the interior peptide bond of Ala_4 is predominantly poly-proline-II-like. The Raman excitation profiles of both Ala_3 and Ala_4 reveal a charge transfer electronic transition at 202 nm, where electron transfer occurs from the terminal nonbonding carboxylate orbital to the adjacent peptide bond π^* orbital. Raman depolarization ratio measurements support this assignment. An additional electronic transition is found in Ala_4 at 206 nm.

Introduction

UV resonance Raman (UVRR) spectroscopy is recognized as a powerful technique for probing peptide and protein secondary structure.[1−14] UVRR spectroscopy also provides insight into the geometry of the excited states and electronic transitions through Raman excitation profiles and Raman depolarization ratios.[11−13] Excitation between 180 and 215 nm is in resonance with the amide $\pi \rightarrow \pi^*$ electronic transition of the peptide backbone, results in enhancement of amide vibrations.[1−13] In the work here, we use UVRR spectroscopy to examine the secondary structure conformations and underlying electronic transitions of both Ala_3 and Ala_4.

Alanine-based peptides are often used as theoretical and experimental models to study protein conformation and folding.[1,2,15−25] The folded state of longer alanine peptides is predominantly α-helix-like,[1−3,19,24,25] while the conformation of the unfolded state has been established to be a polyproline II (PPII)-helix-like structure[9,20−23,26] (although there remains some controversy with this assignment[27,28]). Short alanine peptides, such as trialanine (Ala_3) and tetraalanine (Ala_4), are often used as models for the unfolded state of peptides and proteins. Although there have been numerous studies of Ala_3 and Ala_4 which have identified a number of equilibrium conformations, the conformational distributions are still not clear.[15,29−43]

Most studies agree that the unfolded state for both peptides is populated mainly by the poly-proline II helix (PPII) conformation.[15,29−36,38,41−43] There is, however, little agreement on the other conformations present in equilibrium. The reported conformational distributions include only PPII,[31,39,41,42] PPII with either an additional β structure[29,30,33] or a right-handed α-helix (α_R),[43] and a β structure with an α_R-helix.[15,32,35,36,40] Another study reported that the conformations in solution include PPII, a β-like structure, an α_R-helix, and a γ-turn.[38] A few studies that found only one conformation present assigned it to either a left-handed helix[34] or an extended β-helix-like structure,[37] both of which are similar to a PPII-like conformation.

In the study here, we measured the UVRR excitation profiles and Raman depolarization ratios of aqueous solutions of Ala_3 and Ala_4 between 198 and 210 nm at 25 °C to determine the solution conformation(s) and electronic transitions of Ala_3 and Ala_4. We find that both Ala_3 and Ala_4 adopt three primary conformations—PPII-like, 2.5_1-helix-like, and type II turns—and that Ala_4 may also adopt an additional unknown conformation. We observe the previously described charge transfer transition[12] at 202 nm in both peptides. We also observe a transition in Ala_4 at 206 nm, whose origin remains murky.

Materials and Methods

Sample Preparation. Dialanine (Ala_2), trialanine (Ala_3), and tetraalanine (Ala_4) were purchased from Bachem (Torrance, CA) and used as received. We used 6.6 mM, pH 7 solutions of Ala_3 and Ala_4 for the UVRRS measurements. Each sample contained sodium perchlorate (0.2 M) as an internal standard. The UVRR spectral measurements were taken at 25 ± 0.5 °C.

Raman Instrumentation. The UVRR instrumentation was previously described.[44] The laser source used was a Positive Light Co. Indigo-DUV Ti:sapphire laser system (Coherent, Santa Clara, CA). The Indigo-DUV system utilizes an intracavity frequency doubled, Q-switch pulsed Nd:YLF Evolution 15 laser (527 nm, 30 ns pulse width, 5 kHz repetition rate, 10 W average power) to pump a Ti:sapphire oscillator, which generates tunable radiation from 772 to 840 nm. Raman excitation in the deep UV is obtained by mixing the third harmonic with the fundamental, producing tunable radiation between 193 and 210 nm. The average powers in the deep UV vary between 2 and 5 mW.

The laser beam was focused into a temperature-controlled, circulating flow stream. The flow stream was purged with N_2 to eliminate Raman scattering from the O_2 band at 1555 cm^{-1}. Each 20 mL sample was irradiated for a maximum of 15 min. The scattered light was directed into a subtractive double monochromator,[44] and the Raman scattered light was detected by a liquid nitrogen cooled CCD (Princeton Instruments, Spec-10:400B). The Raman intensities were normalized to that of the 932 cm^{-1} perchlorate (ClO_4^-) symmetric stretch vibration.

* To whom correspondence should be addressed. E-mail: asher@pitt.edu.

10.1021/jp100428n © 2010 American Chemical Society
Published on Web 04/26/2010

The spectra were analyzed and deconvoluted using Grams/32 AI 8.0 software (Thermo Electron Corporation, Waltham, MA).

UV Raman depolarization ratios (ρ) were measured using a 180° back scattering geometry. The light collected from the sample was directed through a UV linear dichroic polarizer (Oriel Instruments, Stratford, CT) followed by a crystalline quartz polarization scrambler (Spex Industries, Edison, NJ) before the monochromator entrance slit. The depolarization ratio ρ was calculated as a ratio of the perpendicular polarized light ($I_\perp$) to the parallel polarized light ($I_{||}$):

$$\rho = \frac{I_\perp}{I_{||}} \quad (1)$$

The depolarization ratios of ClO_4^- and cyclohexane were used as standards[14] to verify the accuracy of the measured depolarization ratios.

Spectrometer Efficiency. The spectrometer used was a modified Spex 1401 double monochromator that operates over the 193−270 nm range. We corrected for the wavelength dependence of throughput efficiency by using previously determined spectrometer efficiencies.[44]

Absorption Measurements. The UV absorption spectra of Ala_2, Ala_3, and Ala_4 between 190 and 250 nm were measured using a Cary 5000 Varian UV−vis-NIR spectrophotometer. The absorption measurements were taken with solution concentrations of 0.5 mM at pH 7 and pH 2 at room temperature (25 ± 0.5 °C).

Results and Discussion

Absorption Spectra. The absorption spectra of Ala_2, Ala_3, and Ala_4 are shown in Figure 1. The molar absorptivities increase for all three peptides at both pH 7 and pH 2 as the wavelength decreases from 250 to 190 nm.

For Ala_2, the broad absorption band centered below ~190 nm derives from the amide $\pi \rightarrow \pi^*$ NV_1 electronic transition for both pH 7 and pH 2 (Figure 1a). The absorption maximum of the pH 2 spectrum, where the carboxylate group is protonated, appears to be blue-shifted compared with the pH 7 spectrum. The pH difference spectrum for Ala_2 indicates the presence of an underlying transition in the pH 7 absorption spectrum at ~202 nm, which disappears at pH 2. The absorption difference spectra for each peptide can be well fit with two Gaussian bands (Figure 2). For Ala_2, the Gaussian bands are centered at 180 nm (not shown) and 203 nm (Figure 2a). The 180 nm band is assigned to the amide NV_1 $\pi \rightarrow \pi^*$ electronic transition, and we assign the ~203 nm band to a charge transfer transition, similar to those previously found in Gly dipeptides.[12] Chen et al.[12] previously demonstrated that a charge transfer transition occurs at ~200 nm in short Gly peptides. The transition involves transfer of charge from the nonbonding carboxylate orbital to the amide π^* orbital (Figure 3). This charge transfer band disappears in the low pH protonated species.

For Ala_3 (Figure 1b) and Ala_4 (Figure 1c), the broad absorption band centered below ~190 nm derives from the amide $\pi \rightarrow \pi^*$ NV_1 electronic transition at both pH 7 and pH 2. The Ala_3 and Ala_4 pH 7 spectra are broader and absorb more than the pH 2 spectra.

UVRR Spectra. The UVRR spectra for Ala_3 and Ala_4 at 25 °C excited between 198 and 210 nm are shown in Figures 4 and 5, respectively. All spectra were normalized to the symmetric perchlorate stretch (932 cm^{-1}).

Vibrations enhanced in both Ala_3 and Ala_4 include the amide I (AmI) vibration at ~1655 cm^{-1}, which is primarily a C═O stretching vibration (st). The enhanced amide II (AmII) vibration involve C−N stretching (st), coupled with N−H bending (b) at ~1550 cm^{-1}. The symmetric stretching of the carboxylate appears at ~1400 cm^{-1} but is overlapped by other bands. The symmetric b vibrations of the CH_3 and C_α−H groups occur at 1371 and 1332 cm^{-1}, respectively. There is an additional vibration present at 1391 cm^{-1} assigned as CH_3 + C_α−H bending, which most strongly overlaps the symmetric carboxylate stretch. The amide III (AmIII) region is broad and spans the 1200−1300 cm^{-1} range. The bands in the AmIII region result primarily from vibrations composed of C−N st coupled to N−H b but can also include C_α−C st, N−C st, C−N st, and some C_α−H b.[9] Both peptides show the highest relative band intensities for 202 nm excitation. The relative band intensities within the spectra are similar across the range of excitation wavelengths, indicating that similar or identical electronic transitions are involved in the enhancement.

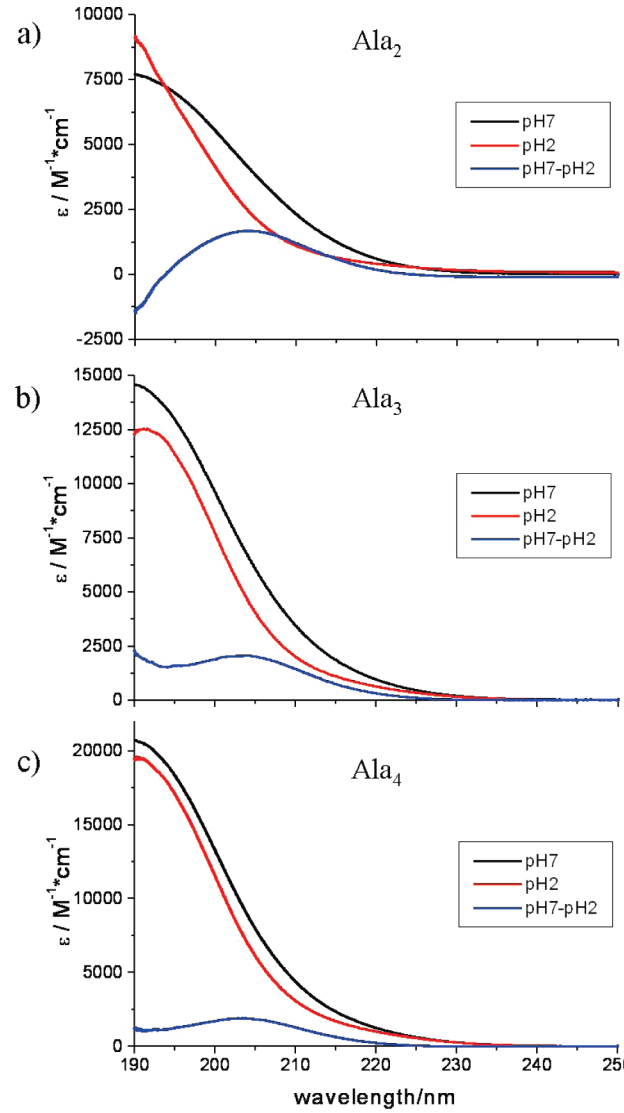

Figure 1. UV absorption spectra at pH 7 (black) and pH 2 (red) and the pH absorption difference spectra (blue) for (a) Ala_2, (b) Ala_3, and (c) Ala_4. All absorption measurements were taken of 0.5 mM peptide solutions at 25 °C.

Our group has previously shown that, for a 21-residue, primarily Ala peptide in mixtures of H_2O/D_2O, the spectra of the partially deuterated chains can be modeled as a statistically weighted linear sum of the deuterated and protonated segments of the peptide.[10,45] This result indicates that the peptide bond

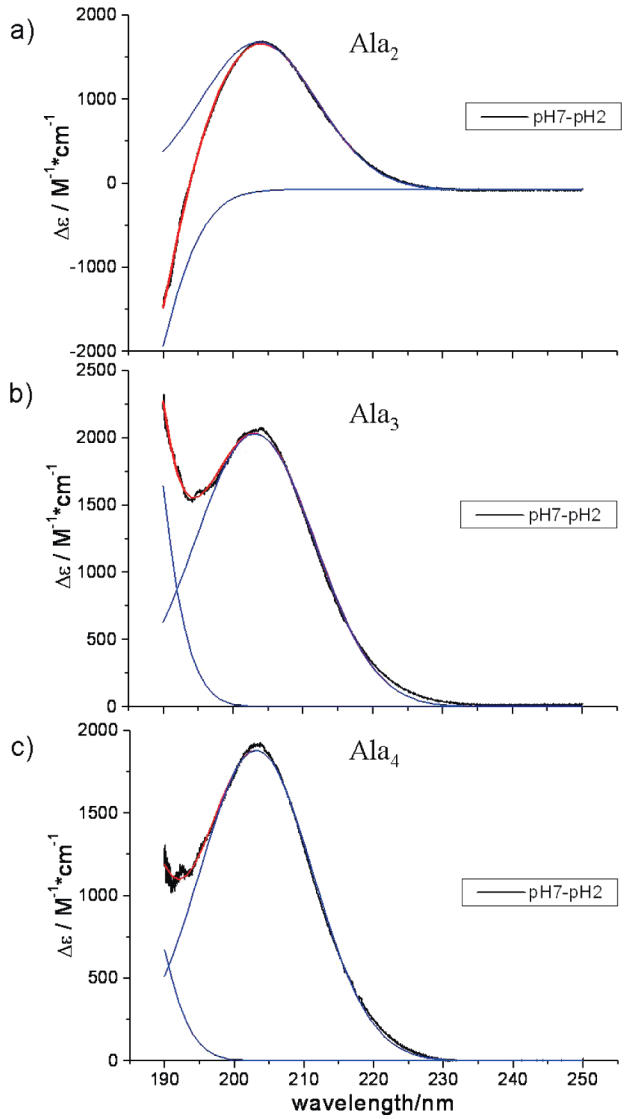

Figure 2. Deconvolution of absorption spectra. The pH 7 − pH 2 difference spectra (black) are fit with two Gaussian bands (blue); the resulting fit curve (red) matches the experimental curve remarkably well: (a) Ala_2, (b) Ala_3, (c) Ala_4.

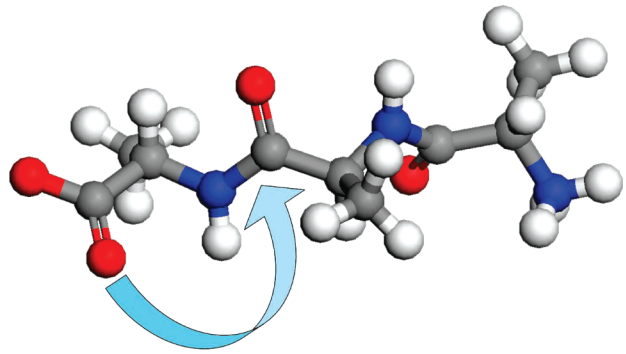

Figure 3. Ala_3 zwitterion in an extended β conformation. The electron density charge transfer from carboxylate to amide is indicated by the blue arrow. (Picture courtesy of Nataliya Myshakina.)

vibrations are localized within the individual peptide bonds. More recently, we also showed that, for short Gly peptides, there is also a lack of coupling between adjacent peptide bond vibrations.[46] These results allow for accurate modeling of the Raman spectra of peptides in solution because the spectra are simply a linear sum of the terminal and internal peptide bonds.

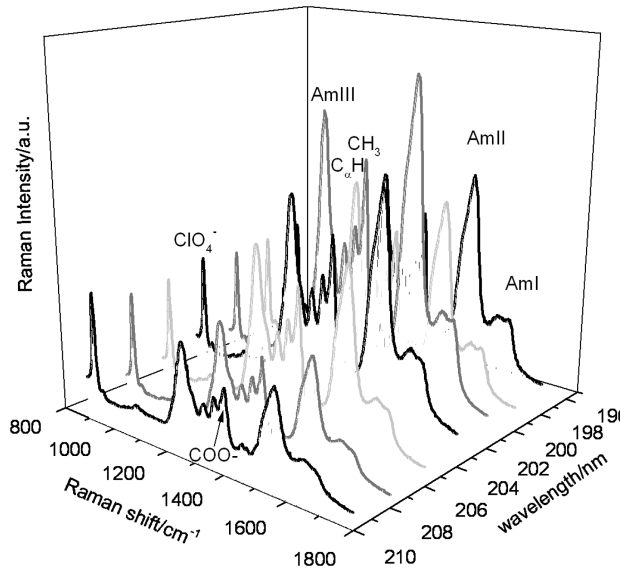

Figure 4. UVRR spectra of Ala_3 (6.6×10^{-3} M) at 25 °C excited between 198 and 210 nm. Spectra were collected for 15 min each. The spectral resolution is ~5 cm^{-1}. Spectra were not corrected for self-absorption or spectrometer throughput efficiency.

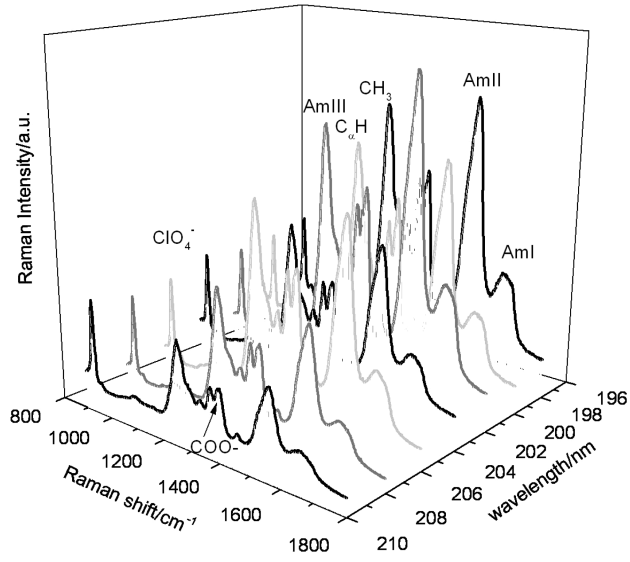

Figure 5. UVRR spectra of Ala_4 (6.6×10^{-3} M) at 25 °C excited between 198 and 210 nm. Spectra were collected for 15 min each. The spectral resolution is ~5 cm^{-1}. Spectra were not corrected for self-absorption or spectrometer throughput efficiency.

The spectra for the terminal and internal peptide bonds significantly differ.[46] We showed that the spectrum of a three-residue peptide approximates the spectrum of the two terminal peptide bonds of an oligopeptide, while the difference spectrum between a six-residue peptide and a five-residue peptide accurately models the spectra of an internal peptide bond. We use this methodology to resolve the spectra of the COO^- vibration for both Ala_3 and Ala_4.

To resolve the COO^- vibration in Ala_3, we assume that the UVRR spectrum of the Ala_3 NH_3^+ end peptide bond is similar to that of the interior peptide bond of Ala_4, which we model as that resulting from subtraction of the Ala_4 − Ala_3 UVRR (Figure 12). The underlying reasoning is that this peptide bond has the standard peptide bond $\pi \rightarrow \pi^*$ transition as the internal peptide bonds, without the charge transfer band of the carboxylate terminal peptide bonds.

We then model the Ala_3 UVRR spectra of the carboxylate end peptide bond as resulting from the UVRR spectral subtraction $Ala_3 - (Ala_4 - Ala_3) = 2*Ala_3 - Ala_4$, where the NH_3^+ end peptide bond UVRR (interior Ala_4 peptide bond spectrum) is subtracted from the Ala_3 spectrum (Figure 6a). This spectral subtraction is obtained using the perchlorate internal standard intensity. This spectrum clearly shows the strong enhancement of the 1405 cm^{-1} carboxylate stretching vibration due to excitation within the charge transfer absorption spectrum.

Identically, we can resolve the Ala_4 COO^- band by the UVRR subtraction $Ala_4 - 2*(Ala_4 - Ala_3) = 2*Ala_3 - Ala_4$, where we assume that the UVRR spectrum of the Ala_3 NH_3^+ end peptide bond is similar to that of the interior Ala_4 peptide bond, which we model as that resulting from subtraction of the $Ala_4 - Ala_3$ UVRR (Figure 6b). The resulting spectrum identically shows the strong Ala_4 enhancement of the 1405 cm^{-1} carboxylate stretching vibration due to excitation within the charge transfer absorption spectrum.

Absolute Raman Cross Sections. To quantitatively compare the spectra across the range of excitation wavelengths, we calculated the Raman cross sections for each amide band at each wavelength, using ClO_4^- as the internal standard. It has been shown that the ClO_4^- symmetric stretching band has an Albrecht A-term frequency dependence for excitation wavelengths from the visible to the UV (to 220 nm).[47] We extrapolated the ClO_4^- cross sections to 198 nm.

The absolute Raman cross sections (with a correction factor for self-absorption) were calculated from

$$\sigma_{peptide} = \frac{I_{band} \cdot k(\lambda_{ClO_4}) \cdot C_{ClO_4} \cdot \sigma_{ClO_4}}{I_{ClO_4} \cdot k(\lambda_{band}) \cdot C_{peptide} \cdot n_A} \cdot \left[\frac{\varepsilon_s + \varepsilon_o}{\varepsilon_r + \varepsilon_o}\right] \quad (2)$$

where I_{band} and I_{ClO_4} are the relative intensities of the amide and ClO_4^- bands, respectively;[4,47] $k(\lambda_{band})$ and $k(\lambda_{ClO_4})$ are the spectrometer efficiencies at the wavelengths of the Raman bands; $C_{peptide}$ and C_{ClO_4} are the concentrations (M) of the individual Ala peptides and perchlorate; σ_{ClO_4} is the calculated ClO_4^- cross section at the band wavelength; n_A is the number of amide bonds in the peptide; ε_o is the molar absorptivity of the peptide at the laser excitation frequency; ε_s is the molar absorptivity of the peptide at the Raman band wavelength; and ε_r is the molar absorptivity at the ClO_4^- band wavelength. The expression in the brackets corrects the measured Raman intensities for self-absorption.[48,49]

These Raman cross sections of the AmI, AmII, AmIII, C_α−H, and CH_3 bends are actually the summed Raman cross sections for each of these Raman bands over all of the peptide bonds, which as we showed previously scatter independently[46] (except for the AmI band of the α-helix conformation). In contrast, only the terminal COO^- peptide bond gives rise to enhancement of the symmetric COO^- stretch. Thus, we evaluated its cross sections from the difference spectra obtained, as shown in Figure 6.

Excitation Profiles. The excitation profiles for Ala_3 shown in Figure 7 indicate that the Raman cross sections increase as the excitation wavelength decreases from 210 nm to maxima at 202 nm. It is well-established that the NV_1 $\pi \rightarrow \pi^*$ electronic transitions in short peptides occur at or below 190 nm (Figure 1).[50−52] The excitation profile maxima at 202 nm occur close to the maximum wavelength of the charge transfer transition found in the pH difference absorption spectrum of Ala_3.

Examination of the Figure 7 Ala_3 excitation profiles indicates that the largest cross sections occur for the AmII vibration,

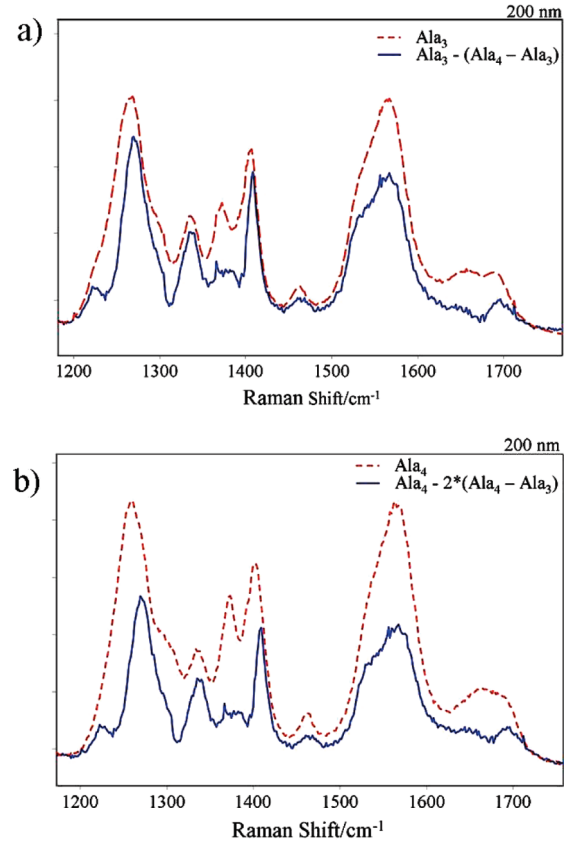

Figure 6. Resolving the carboxylate stretching vibration in 200 nm excited (a) Ala_3: measured spectrum (red) and $Ala_3 - (Ala_4 - Ala_3)$ difference spectra (blue) showing COO^- vibration enhanced in COO^- end peptide bond. (b) Ala_4: measured spectrum (red) and $Ala_4 - 2*(Ala_4 - Ala_3)$ difference spectra (blue) showing COO^- vibration enhanced in COO^- end peptide bond.

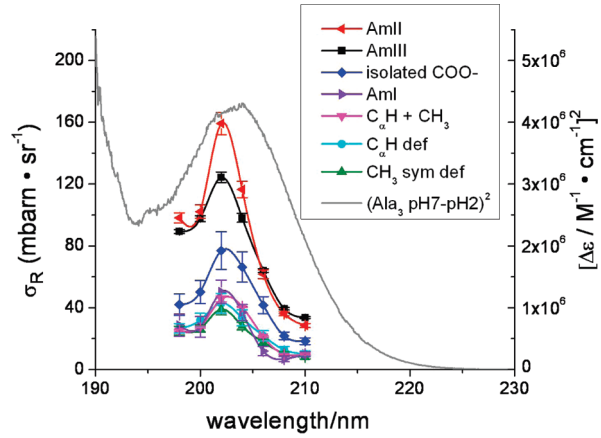

Figure 7. Absolute Raman cross section excitation profiles of Ala_3 (mbarn/sr) between 198 and 210 nm. See text for details. Also shown is the squared pH absorption difference spectrum from Figure 2. The isolated COO^- excitation profile was calculated using the $Ala_3 - (Ala_4 - Ala_3)$ difference spectra shown in Figure 6.

which is mainly a C−N st coupled to an N−H b. A similar maximal AmII band enhancement is also seen in the longer, 21-residue alanine peptide (AP).[4] The next largest cross section occurs for the AmIII vibration, which is also composed of a C−N st and N−H b. The AmIII cross section in AP was also found to be less than that of the AmII.[4] Normal mode calculations of polyalanine indicate that C−N motion contributes twice as much to the AmII vibration than to the AmIII vibration.[53] The COO^- symmetric stretch shows the next largest

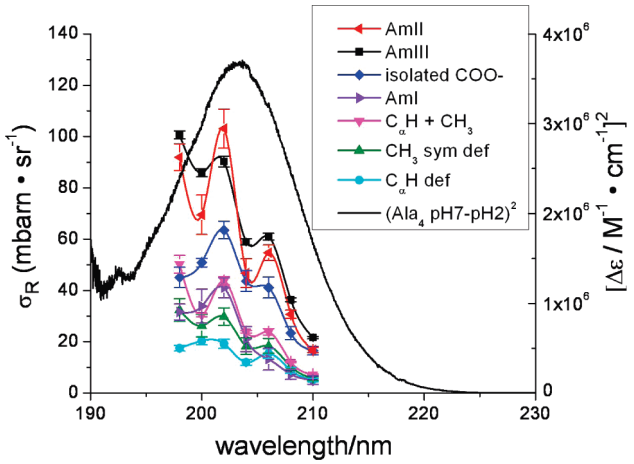

Figure 8. Absolute Raman cross section excitation profiles of Ala_4 (mbarn/sr) between 198 and 210 nm. See text for details. Also shown is the squared pH absorption difference spectrum from Figure 2. The isolated COO− profile was calculated using the $Ala_4 - 2*(Ala_4 - Ala_3)$ difference spectra shown in Figure 6.

excitation profile cross section.[12] The COO^- symmetric st is selectively enhanced by the ~202 nm charge transfer transition.[12]

All of the excitation profiles are much narrower than the charge transfer absorption difference spectra. The resonance Raman cross sections of CH_3, $C_\alpha H$, and AmI vibrations are significantly smaller with only a modest charge transfer enhancement.

The Raman excitation profiles for Ala_4 shown in Figure 8 differ significantly from those of Ala_3 in that they show two distinct maxima. There are two peptide bonds in Ala_3, whereas Ala_4 contains three. The AmII and AmIII vibrations once again have the largest cross sections, with the AmIII vibration having a significantly larger relative cross section than in Ala_3. The AmI band cross section per peptide bond at 202 nm is approximately twice that in Ala_3.

As the excitation wavelength decreases from 210 to 198 nm, a small excitation profile maximum is observed at 206 nm, followed by a larger maximum at 202 nm. The excitation profile maximum at 202 nm for Ala_4 is assumed to be due to the charge transfer transition in the pH difference absorption spectrum (Figures 1c and 2c), while understanding the origin of the 206 nm maximum will require additional information. It is important to note that the cross sections per peptide bond are roughly similar between Ala_3 and Ala_4 (except for the AmI) but the peak values are smaller in Ala_4, while the excitation profiles appear broader than those of Ala_3.

The lowest order theory[54] indicates that the resonance Raman excitation profiles will scale as the square of the absorbance band molar absorptivity. Figures 7 and 8 also compare the excitation profiles of Ala_3 and Ala_4 to the squares of their absorption difference spectra. This comparison shows more similar bandwidths.

The COO^- symmetric st is clearly visible for short peptides such as Ala_3 and Ala_4. However, the COO^- symmetric st will be less evident in longer peptides such as AP, where the peptide bond NV_1 $\pi \rightarrow \pi^*$ transitions dominate the excitation profile, resulting in a small relative enhancement of the COO^- symmetric st.

Raman Depolarization Ratios, Excitation Profiles, and Absorption Spectra. In order to gain insight into the origin of the excitation profiles, we measured the dispersions of the resonance Raman depolarization ratios. Figure 9 compares the

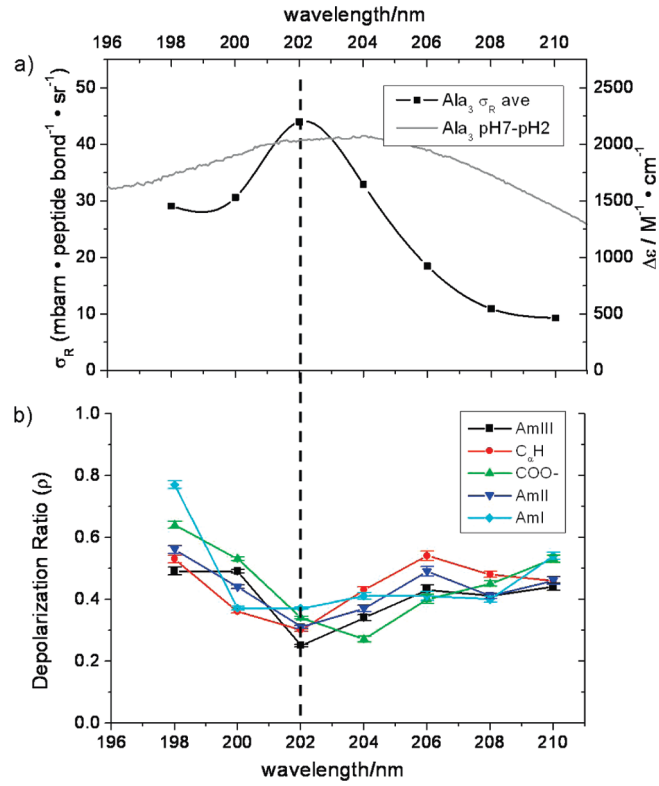

Figure 9. (a) Average Raman excitation profile for the Ala_3 amide bands at 25 °C between 198 and 210 nm and the pH 7 − pH 2 absorption difference spectrum of Ala_3 at 25 °C between 196 and 212 nm. (b) Raman depolarization ratios of Ala_3 at 25 °C. The dashed line indicates the coincidence between the excitation maximum of the excitation profile, the pH absorption difference spectrum, and the depolarization ratio minimum with $\rho \approx 0.33$ at 202 nm.

Ala_3 absorption difference spectrum, the Raman excitation profile averaged over the enhanced vibrations and the Raman depolarization ratios. The excitation profile is slightly blue-shifted and much narrower than the absorption difference spectrum.

The Ala_3 depolarization ratio shows a minimum of ρ ~0.33 at the excitation profile maximum, indicating that a single nondegenerate electronic transition, presumably the charge transfer transition, dominates the resonance Raman enhancement at 202 nm.[4,12,13,55] At excitation wavelengths above and below the excitation profile maximum, $\rho > 0.33$, indicating contributions of additional electronic transitions.[4,12,13,55] This excitation profile behavior, where $\rho > 0.33$ for preresonance excitation and also $\rho > 0.33$ from 201 to 198 nm, between the charge transfer transition and the NV_1 transition, is not possible if the 202 nm transition and the NV_1 are the only transitions involved in enhancement. There is a hint of another transition at 206 nm evidenced by the skewed Raman excitation profile.

Figure 10 shows the Ala_4 pH absorption difference spectrum, the average resonance Raman excitation profile, and the depolarization ratio dispersion measurements. The Ala_4 excitation profile shows a second maximum at 206 nm, ~1000 cm^{-1} lower in frequency than that of the ~202 nm charge transfer transition. As observed for Ala_3, a global depolarization minimum occurs with ρ ~0.33 at the charge transfer excitation profile maximum at 202 nm. Also, as for Ala_3, $\rho > 0.33$ from 201 to 198 nm, between the charge transfer transition and the NV_1 transition at ~190 nm. In contrast to Ala_3, a local depolarization ratio maximum occurs at the 206 nm second excitation profile maximum (ρ ~0.5). $\rho > 0.33$ in preresonance

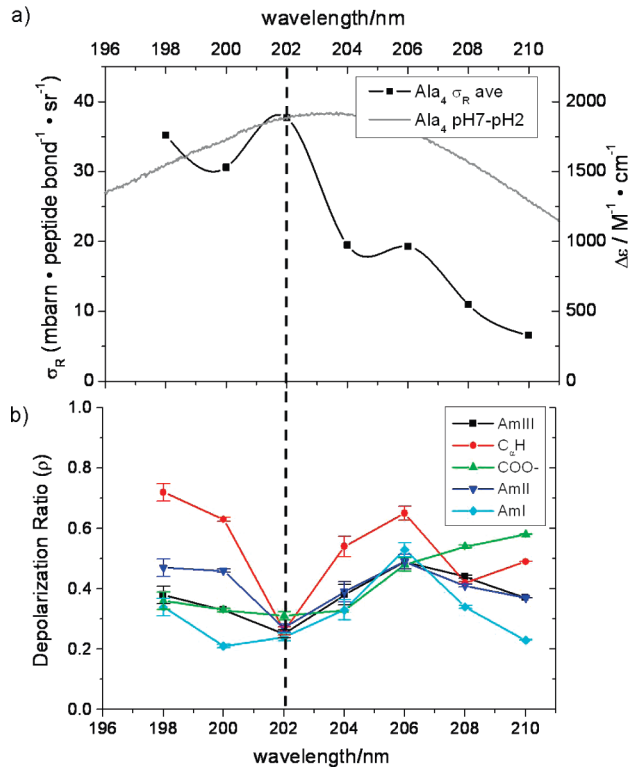

Figure 10. (a) Averaged Raman excitation profile for Ala_4 at 25 °C between 198 and 210 nm and the pH 7 − pH 2 absorption difference spectrum of Ala_4 at 25 °C from 196 to 212 nm. (b) Raman depolarization ratios of Ala_4 at 25 °C. The dashed line indicates the coincidence between the maximum of the excitation profile, the pH absorption difference spectrum, and the depolarization ratio minimum with $\rho \approx 0.33$ at 202 nm.

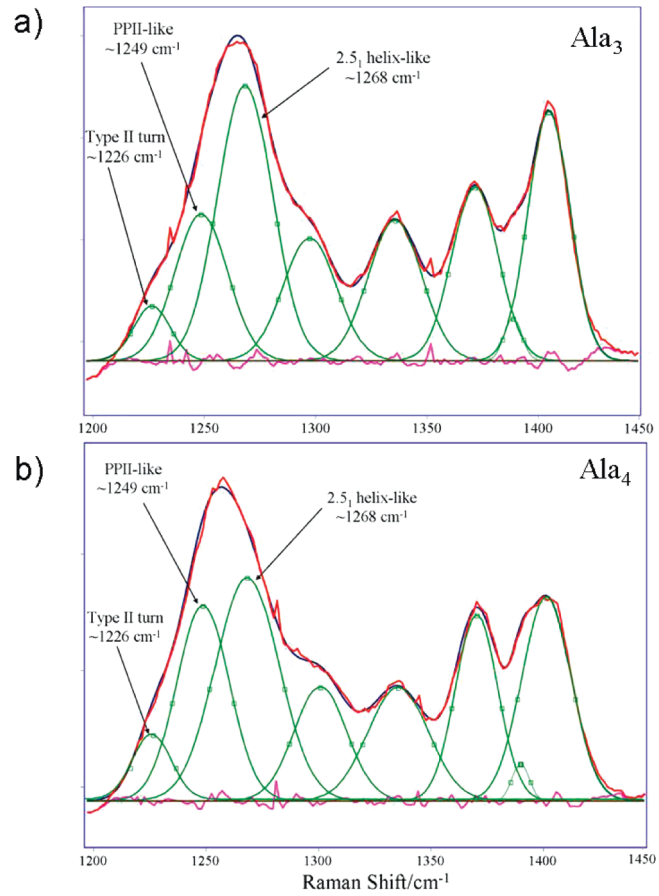

Figure 11. (a) Deconvolution of the Ala_3 $AmIII_3$ region excited at 204 nm with three Gaussian bands. (b) Deconvolution of the Ala_4 $AmIII_3$ region excited at 204 nm, also with three Gaussian bands. Different conformational distributions are present. There is excellent agreement between the modeled peaks and the observed data ($R^2 > 99\%$).

with all of these transitions for the carboxylate stretch and the AmII and III bands (although less so than for Ala_3).

We do not, as yet, have a simple explanation for these results. One possibility would require two charge transfer transitions close in energy that give rise to the two excitation profile peaks in Ala_4 and the very weak 206 nm shoulder in Ala_3. These charge transfer transitions would involve two different sets of carboxylate nonbonding electrons undergoing a transition to the adjacent peptide bond π^* orbital. The weakness of the 206 nm excitation profile maximum in Ala_3 could result from destructive interference between the contributions from these two charge transfer transitions and the NV_1 transition. Although the observed 206 nm Raman intensities could be dramatically attenuated by the destructive interference, the 206 nm transition could still significantly increase ρ in the wings of the excitation profile maxima.

The dispersion of ρ can be understood if the contribution to the polarizability of the NV_1 transition and the 202 nm charge transfer transition were of the same sign and the 206 nm transition contribution were of opposite sign. This would yield the dispersion observed with $\rho > 0.33$ between 201 and 198 nm, if the NV_1 transition and the 202 nm charge transfer transition dominated in this spectral region and the NV_1 transition and the 202 nm charge transfer transition contributed similarly to that of the 206 nm transition.

The alternative explanation would assign the 206 and 202 nm transitions to the 0−0 and 0−1 vibronic components of the charge transfer transition. The ~1000 cm^{-1} difference in the peak maxima would indicate a decreased excited state carboxylate frequency. A detailed theoretical calculation would be required to understand the dispersion of the depolarization ratios around the 206 nm transition.[56]

Another possible origin of the 206 nm band is that the second conformation of the Ala_4 peptide occurs in solution, which has its charge transfer transition shifted to 206 nm. To search for evidence for this additional conformation, we examined the AmIII region, which is sensitive to the peptide bond conformations.[7]

Deconvolution of the AmIII Region. We deconvoluted the $AmIII_3$ region in both Ala_3 and Ala_4 (Figure 11) and found that the $AmIII_3$ region could be well fit with three Gaussian bands, at ~1226, 1249, and 1268 cm^{-1}. We utilized the methodology of Mikhonin et al.[7] which correlates Raman $AmIII_3$ frequency to Ψ angle, specifically using their eq 6A which is applicable to peptide bonds fully exposed to water, such as in poly-proline II (PPII) helix, 2.5_1 helix, extended β-strand conformations, and certain turn structures. The deconvoluted peak positions correlate to the following Ψ angles: ~ +120°, ~ +150°, ~ +170°, which most likely derive from type II turns, PPII-helix-like, and 2.5_1-helix-like conformations, respectively. The Ψ angle of 120° is also found for type VIa and type VIII turns; however, these are less likely structures to occur. Also, note that the Raman frequencies correspond only to Ψ angle values, with no information about the Φ angle. Thus, there are structures with type II turn Ψ angles, but it is possible that a significant Φ angle variation could be present. Comparing Figure 11a and b, assuming identical Raman cross sections for these species, we find that the relative contribution of the 2.5_1-helix-like structure

in Ala_4 is less than that in Ala_3, and conversely, the PPII-helix-like contribution is larger in Ala_4 than in Ala_3.

Assuming identical Raman cross sections per peptide bond for each conformation, we can roughly estimate the population distributions from the $AmIII_3$ bands of both peptides. We find that the relative population distributions of both peptides are independent of wavelength. For Ala_3, the type II turn has the lowest relative contribution (~8%), the PPII-like conformation contribution is ~29%, and the 2.5_1 helix contribution is ~63%.

Although there have been numerous theoretical and experimental studies performed on Ala_3 using a variety of techniques, there is no existing consensus on the conformational distribution for Ala_3 in solution. Most studies agree that Ala_3 occurs in a PPII-like conformation.[15,29−36,38,41−43] Other possible conformations include β-sheet-like,[29] β-strand,[15,30] β structures,[32,33,35,36,38,43] right-handed α-helix,[15,33,35,36,38,43] and γ-turn.[38] No previous study identified the 2.5_1 helix conformation, although there is a suggestion of an extended β-strand-like conformation with a similar Ψ angle (~170°).[15,37]

For Ala_4, the conformations found are similar to those in Ala_3, although the distribution is different. There is a larger contribution from the PPII-helix-like structure (39%). The type II turn contribution is similar (8.5%), while the 2.5_1 helix contribution is less than that in Ala_3 (52%). Garcia[57] determined that four consecutive amino acid residues are required to form a water stabilized PPII structure, lending support to the result that Ala_4 should show a larger contribution from PPII-like structures than Ala_3. Again, there is little consensus on the conformational distribution in Ala_4, although there is agreement that the peptide adopts both PPII-like and β-like structure,[39,40] with a small amount of a right-handed α-helix-like conformation.[40] We assign the 202 nm excitation maximum as the charge transfer transition for all three conformations of Ala_4. None of these conformations should obviously give rise to a shifted 206 nm charge transfer band.

Ala_4 and Ala_3 Difference Spectra. To differentiate the conformational distribution of the internal versus terminal peptide bonds of Ala_4, we examined the $Ala_4 - Ala_3$ difference spectrum (Figure 12a), which models the internal Ala_4 peptide bond UVRR by removing the contribution of the terminal carboxylate and amine groups. We note that the COO^- symmetric stretching vibration is absent in the difference spectra. The contributions of the carboxyl end group of both peptides were removed by this subtraction. The relative intensities and frequencies of the bands within each spectrum are similar across the range of excitation wavelengths, once again indicating similar enhancement of the bands.

We calculated the Raman cross sections of the $AmIII_3$ bands (Figure 12b). We find that the internal residue of Ala_4 is predominantly PPII-like (~72%), with smaller contributions from 2.5_1 helix (19%) and type II turn structures (~9%). A previous MD simulation study on the middle residue of Ala_3 found that it was ~85% PPII-like,[31] which closely agrees with our findings here. We can also infer that the 2.5_1-helix-like conformation is largely found at the peptide ends, which could be representative of a less compact structure at the peptide terminal ends.

An interesting feature in the excitation profiles of $Ala_4 - Ala_3$ is that the 202 and 206 nm excitation profile maxima are present for both the PPII-like and 2.5_1 helix conformation profiles, but less evident in the type II turn profiles. Thus, as expected, we see less contribution from the charge transfer enhancement in the estimated excitation profile of the internal peptide bond. This residual enhancement may result because our assumption that the difference spectrum results completely from the Ala_4 internal peptide bond is not completely accurate.

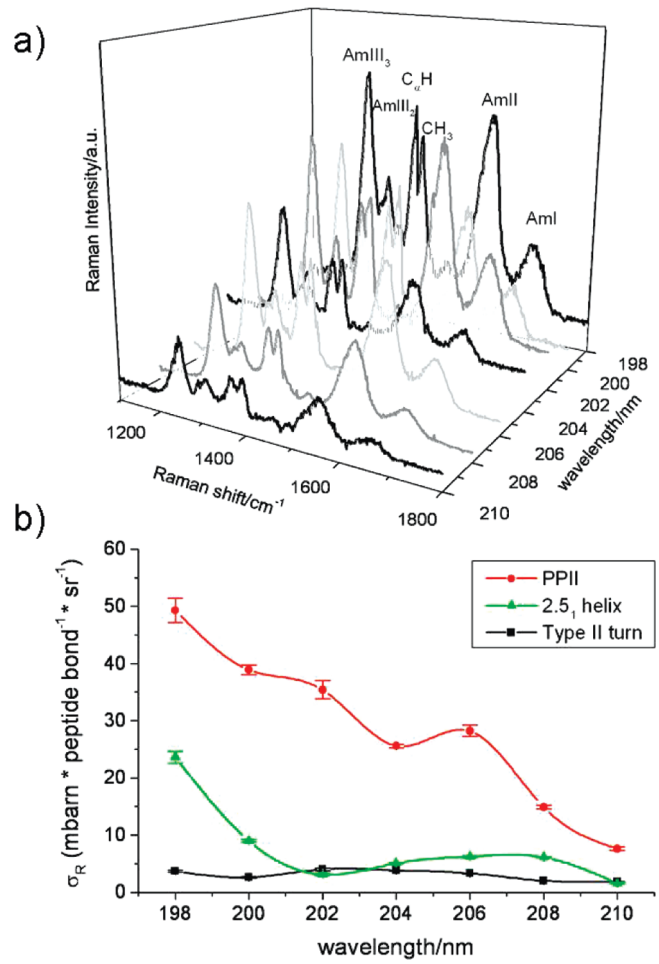

Figure 12. (a) $Ala_4 - Ala_3$ difference spectra, from 198 to 210 nm. (b) The $AmIII_3$ band Raman cross sections of the three conformations (type II turn, PPII-helix-like, 2.5_1 helix) in the $Ala_4 - Ala_3$ difference spectra.

Conclusions

We measured the Raman excitation profiles and depolarization ratios for both Ala_3 and Ala_4. Both peptides show excitation profile maxima at 202 nm, which we assign to charge transfer transitions of the carboxylate terminated peptide bonds clearly observed in the pH absorption difference spectra. Ala_4 shows an additional smaller excitation profile maximum at 206 nm whose origin remains unclear.

We correlated the $AmIII_3$ band Raman frequencies to the Ψ angle of both Ala_3 and Ala_4 to determine the conformational distribution of these peptides. We found type II turns, as well as PPII-like and 2.5_1 helix-like conformations in solution. The $Ala_4 - Ala_3$ Raman difference spectra allowed us to separately study the interior peptide bond of Ala_4, which is found to be predominantly PPII-like.

We assign the charge transfer transition at 202 nm to the three β-type structures deconvoluted from the Raman spectra. We are also able to resolve the COO^- vibration for both Ala_3 and Ala_4. We find a shoulder in the Ala_4 excitation profile at 206 nm but are unable at this time to definitively assign its origin.

Acknowledgment. We would like to thank Prof. John A. Shelnutt for a very helpful discussion and Dr. Nataliya My-

shakina for providing the image for Figure 3. We thank the NIH for funding, Grant Nos. 5R01EB002053 and 1R01EB009089.

References and Notes

(1) Ianoul, A.; Mikhonin, A.; Lednev, I. K.; Asher, S. A. *J. Phys. Chem. A* **2002**, *106*, 3621.
(2) Lednev, I. K.; Karnoup, A. S.; Sparrow, M. C.; Asher, S. A. *J. Am. Chem. Soc.* **1999**, *121*, 8074.
(3) Mikhonin, A. V.; Asher, S. A. *J. Am. Chem. Soc.* **2006**, *128*, 13789.
(4) Sharma, B.; Bykov, S. V.; Asher, S. A. *J. Phys. Chem. B* **2008**, *112*, 11762.
(5) Myshakina, N. S.; Ahmed, Z.; Asher, S. A. *J. Phys. Chem. B* **2008**, *112*, 11873.
(6) Efremov, E. V.; Ariese, F.; Gooijer, C. *Anal. Chim. Acta* **2008**, *606*, 119.
(7) Mikhonin, A. V.; Bykov, S. V.; Myshakina, N. S.; Asher, S. A. *J. Phys. Chem. B* **2006**, *110*, 1928–1943.
(8) Mikhonin, A. V.; Myshakina, N. S.; Bykov, S. V.; Asher, S. A. *J. Am. Chem. Soc.* **2005**, *127*, 7712.
(9) Mikhonin, A. V.; Ahmed, Z.; Ianoul, A.; Asher, S. A. *J. Phys. Chem. B* **2004**, *108*, 19020.
(10) Mix, G.; Schweitzer-Stenner, R.; Asher, S. A. *J. Am. Chem. Soc.* **2000**, *122*, 9028.
(11) Pajcini, V.; Asher, S. A. *J. Am. Chem. Soc.* **1999**, *121*, 10942.
(12) Chen, X. G.; Li, P.; Holtz, J. S. W.; Chi, Z.; Pajcini, V.; Asher, S. A.; Kelly, L. A. *J. Am. Chem. Soc.* **1996**, *118*, 9705.
(13) Chen, X. G.; Asher, S. A.; Schweitzer-Stenner, R.; Mirkin, N. G.; Krimm, S. *J. Am. Chem. Soc.* **1995**, *117*, 2884.
(14) DeVito, V. L.; Cai, M. Z.; Asher, S. A.; Kehres, L. A.; Smith, K. M. *J. Phys. Chem.* **1992**, *96*, 6917.
(15) Tsai, M.; Xu, Y.; Dannenberg, J. J. *J. Phys. Chem. B* **2009**, *113*, 309–318.
(16) Imamura, H.; Kato, M. *Proteins: Struct., Funct., Bioinf.* **2009**, *75*, 911.
(17) Wang, W.-Z.; Lin, T.; Sun, Y.-C. *J. Phys. Chem. B* **2007**, *111*, 3508.
(18) Quapp, W *J. Comput. Chem.* **2007**, *28*, 1834.
(19) Morozov, A. N.; Lin, S. H. *J. Phys. Chem. B* **2006**, *110*, 20555.
(20) Zagrovic, B.; Lipfert, J.; Sorin, E. J.; Millett, I. S.; van Gunsteren, W. F.; Doniach, S.; Pande, V. S *Proc. Natl. Acad. Sci. U.S.A.* **2005**, *102*, 11698.
(21) Chen, K.; Liu, Z.; Zhou, C.; Shi, Z.; Kallenbach, N. R. *J. Am. Chem. Soc.* **2005**, *127*, 10146.
(22) Ramakrishnan, V.; Ranbhor, R.; Durani, S. *J. Am. Chem. Soc.* **2004**, *126*, 16332.
(23) McColl, I. H.; Blanch, E. W.; Hecht, L.; Kallenbach, N. R.; Barron, L. D. *J. Am. Chem. Soc.* **2004**, *126*, 5076.
(24) Huang, C.-Y.; Klemke, J. W.; Getahun, Z.; DeGrado, W. F.; Gai, F. *J. Am. Chem. Soc.* **2001**, *123*, 9235.
(25) Thompson, P. A.; Eaton, W. A.; Hofrichter, J. *Biochemistry* **1997**, *36*, 9200.
(26) Gnanakaran, S.; Garcia, A. E. *Proteins: Struct., Funct., Bioinf.* **2005**, *59*, 773.
(27) Vila, J. A.; Baldoni, H. A.; Ripoll, D. R.; Ghosh, A.; Scheraga, H. A. *Biophys. J.* **2004**, *86*, 731.
(28) Makowska, J.; Rodziewicz-Motowidlo, S.; Baginska, K; Makowski, M.; Vila, J. A.; Liwo, A.; Chmurzynski, L.; Scheraga, H. A. *Biophys. J.* **2007**, *92*, 2904.
(29) Eker, F.; Cao, X.; Nafie, L.; Schweitzer-Stenner, R. *J. Am. Chem. Soc.* **2002**, *124*, 14330.
(30) Eker, F.; Griebenow, K.; Schweitzer-Stenner, R. *J. Am. Chem. Soc.* **2003**, *125*, 8178.
(31) Gnanakaran, S.; Garcia, A. E. *J. Phys. Chem. B* **2003**, *107*, 12555.
(32) Gorbunov, R. D.; Nguyen, P. H.; Kobus, M.; Stock, G. *J. Chem. Phys.* **2007**, *126*, 054509/1.
(33) Graf, J.; Nguyen, P. H.; Stock, G.; Schwalbe, H. *J. Am. Chem. Soc.* **2007**, *129*, 1179.
(34) Lee, O.; Roberts, G. M.; Diem, M. *Biopolymers* **1989**, *28*, 1759.
(35) Mu, Y.; Kosov, D. S.; Stock, G. *J. Phys. Chem. B* **2003**, *107*, 5064.
(36) Mu, Y.; Stock, G. *J. Phys. Chem. B* **2002**, *106*, 5294.
(37) Schweitzer-Stenner, R. *Biophys. J.* **2002**, *83*, 523.
(38) Schweitzer-Stenner, R. *J. Phys. Chem. B* **2009**, *113*, 2922.
(39) Schweitzer-Stenner, R.; Eker, F.; Griebenow, K.; Cao, X.; Nafie, L. A. *J. Am. Chem. Soc.* **2004**, *126*, 2768.
(40) Torii, H. *J. Phys. Chem. B* **2007**, *111*, 5434.
(41) Woutersen, S.; Hamm, P. *J. Phys. Chem. B* **2000**, *104*, 11316.
(42) Woutersen, S.; Hamm, P. *J. Chem. Phys.* **2001**, *114*, 2727.
(43) Woutersen, S.; Pfister, R.; Hamm, P.; Mu, Y.; Kosov, D. S.; Stock, G. *J. Chem. Phys.* **2002**, *117*, 6833.
(44) Bykov, S.; Lednev, I.; Ianoul, A.; Mikhonin, A.; Munro, C.; Asher, S. A. *Appl. Spectrosc.* **2005**, *59*, 1541.
(45) Mikhonin, A. V.; Asher, S. A. *J. Phys. Chem. B* **2005**, *109*, 3047.
(46) Dudik, J. M.; Johnson, C. R.; Asher, S. A. *J. Chem. Phys.* **1985**, *82*, 1732.
(47) Ludwig, M.; Asher, S. A. *Appl. Spectrosc.* **1988**, *42*, 1458.
(48) Shriver, D. F.; Dunn, J. B. R. *Appl. Spectrosc.* **1974**, *28*, 319.
(49) Bykov, S. V.; Asher, S. A. *J. Phys. Chem. Lett.* **2010**, *1*, 269.
(50) Basch, H.; Robin, M. B.; Kuebler, N. A. *J. Chem. Phys.* **1967**, *47*, 1201.
(51) Peterson, D. L.; Simpson, W. T. *J. Am. Chem. Soc.* **1957**, *79*, 2375.
(52) Schellman, J. A.; Nielsen, E. B. *J. Phys. Chem.* **1967**, *71*, 3914.
(53) Lee, S.-H.; Krimm, S. *Biopolymers* **1998**, *46*, 283.
(54) Myers, A. B.; Mathies, R. A. In *Resonance Raman Spectra of Polyenes and Aromatics*; Spiro, T. G., Ed.; Biological Applications of Raman Spectroscopy, Vol. 2; John Wiley & Sons: New York, 1987; pp 1−58.
(55) Long, D. A. *The Raman Effect: A Unified Treatment of the Theory of Raman Scattering by Molecules*; John Wiley & Sons: New York, 2001.
(56) Shelnutt, J. A.; O'Shea, D. C. *J. Chem. Phys.* **1978**, *69*, 5361.
(57) Garcia, A. E. *Polymer* **2004**, *45*, 669.

JP100428N